

# Long term $\gamma$ -ray variability of blazars

Bhoomika Rajput<sup>1</sup>, C. S. Stalin<sup>1</sup>, and Suwendu Rakshit<sup>2</sup>

<sup>1</sup> Indian Institute of Astrophysics, Koramangala, Bangalore 560034, India  
e-mail: bhoomika@iiap.res.in

<sup>2</sup> Finnish Centre for Astronomy with ESO (FINCA), University of Turku, Vesilinnantie 5, 20014 Quantum, Finland

Received 24 September 2019 / Accepted 25 December 2019

## ABSTRACT

We used the data from the *Fermi* Gamma-ray Space Telescope to characterise the  $\gamma$ -ray flux variability of blazars on month-like time scales. Our sample consists of 1120 blazars of which 481 are flat spectrum radio quasars (FSRQs) and 639 are BL Lac objects (BL Lacs). We generated monthly binned light curves of our sample for a period of approximately nine years from 2008 August to 2017 December and quantified variability by using excess variance ( $F_{\text{var}}$ ). On month-like time scales, 371/481 FSRQs are variable (80%), while only about 50% (304/639) of BL Lacs are variable. This suggests that FSRQs are more variable than BL Lac objects. We find a mean  $F_{\text{var}}$  of  $0.55 \pm 0.33$  and  $0.47 \pm 0.29$  for FSRQs and BL Lacs respectively. Large  $F_{\text{var}}$  in FSRQs is also confirmed from the analysis of the ensemble structure function. By Dividing our sample of blazars based on the position of the synchrotron peak in their broad-band spectral energy distribution, we find that the low synchrotron peaked (LSP) sources have the largest mean  $F_{\text{var}}$  value of  $0.54 \pm 0.32$  while the intermediate synchrotron peaked (ISP) and high synchrotron peaked sources have mean  $F_{\text{var}}$  values of  $0.45 \pm 0.25$  and  $0.47 \pm 0.33$  respectively. On month-like time scales, we find FSRQs to show a high duty cycle (DC) of variability of 66% relative to BL Lacs that show a DC of 36%. We find that both the  $F_{\text{var}}$  and time scale of variability ( $\tau$ ) do not correlate with  $M_{\text{BH}}$ . We note that  $F_{\text{var}}$  is found to be weakly correlated with Doppler factor ( $\delta$ ) and  $\tau$  is also weakly correlated with  $\delta$ . Most of the sources in our sample have  $\tau$  of the order of days, which might be related to processes in the jet. We find marginal difference in the distribution of  $\tau$  between FSRQs and BL Lacs.

**Key words.** galaxies: active – BL Lacertae objects: general – quasars: supermassive black holes

## 1. Introduction

Flux variability which involves non-periodic changes in flux occurring with different amplitudes and time scales is one of the defining characteristics of active galactic nuclei (AGN) and it was recognised in these objects soon after their discovery about half a century ago (Matthews & Sandage 1963). Blazars are a peculiar category of radio-loud AGN, with bolometric luminosity as large as  $10^{48}$  erg s<sup>-1</sup> or  $10^{14} L_{\odot}$  where their relativistic jets are pointed close to the line of sight to the observer (Urry & Padovani 1995). They are copious emitters of high-energy radiation and show rapid and large amplitude flux variations over the entire accessible spectral region from low-energy radio to high-energy  $\gamma$ -rays (Ulrich et al. 1997). They dominate the extragalactic  $\gamma$ -ray sky as revealed by both the Compton Gamma Ray Observatory (Hartman et al. 1999) and the *Fermi* Gamma Ray Space Telescope (The *Fermi*-LAT Collaboration 2019). Blazars comprise both flat spectrum radio quasars (FSRQs) and BL Lacertae objects (BL Lacs). While FSRQs have broad emission lines in their optical spectra, BL Lacs have either a featureless optical spectra or optical spectra with weak (equivalent width  $< 5 \text{ \AA}$ ) emission lines. Alternatively, Ghisellini et al. (2011) propose a more physical distinction between FSRQs and BL Lacs which is based on the luminosity of the broad line region ( $L_{\text{BLR}}$ ) relative to the Eddington luminosity ( $L_{\text{Edd}}$ ), where  $L_{\text{Edd}} = 1.38 \times 10^{38} (M_{\text{BH}}/M_{\odot}) \text{ erg s}^{-1}$ , and  $M_{\text{BH}}$  is the mass of the black hole. FSRQs with  $L_{\text{BLR}}/L_{\text{Edd}} > 5 \times 10^{-5}$  are believed to be the beamed counterparts of the more luminous Fanaroff & Riley type II (FR II; Fanaroff & Riley 1974) radio sources,

while BL Lacs are the beamed counterparts of the less luminous FRI type radio sources. The broad-band spectral energy distribution (SED) of blazars in the  $\log \nu F_{\nu} - \log \nu$  representation has a two-component structure, with the low-energy component covering the radio to the ultraviolet (UV) and X-ray. The structure is explained by synchrotron emission processes and the high-energy component (covering X-ray to  $\gamma$ -ray), which is explained by inverse Compton emission processes from relativistic electrons in their jets. Based on the location of the peak ( $\nu_p$ ) of the synchrotron emission in their broad-band SED, blazars are further divided into low synchrotron peaked blazars with  $\nu_p < 10^{14}$  Hz, intermediate synchrotron peaked blazars with  $10^{14} \text{ Hz} \leq \nu_p \leq 10^{15}$  Hz, and high synchrotron peaked (HSP) blazars with  $\nu_p > 10^{15}$  Hz. The majority of the FSRQs belong to the LSP category, while a large fraction of HSP sources are BL Lacs.

Since the jets in blazars are aligned close to the observer in the beaming model, the observed emission ( $S_{\text{obs}}$ ) from the jet is Doppler boosted relative to what is measured in the co-moving frame of the jet ( $S_{\text{int}}$ ) as  $S_{\text{obs}} = S_{\text{int}} \delta^q$  (Lin et al. 2017) where  $q = 2 + \alpha$  for a stationary jet and  $q = 3 + \alpha$  for a jet with distinct blobs,  $\alpha$  is the spectral index defined as  $S_{\nu} \propto \nu^{-\alpha}$ ,  $\delta$  is the Doppler factor given by  $\delta = [\Gamma(1 - \beta \cos \theta)]^{-1}$ , where  $\Gamma = (1 - \beta^2)^{-1/2}$  is the bulk Lorentz factor,  $\theta$  is the angle between the observer's line of sight and the jet axis and  $\beta = v/c$  is the jet speed. In addition to flux enhancement, the observed time scale of variability is also shortened by a factor  $\delta^{-1}$ , which is relative to that of the co-moving frame. These two effects increase our chances of detecting variations in blazars over a range of

time scales and amplitudes. Characterising the minimum time scale of variability ( $t_{\min}$ ) from blazar light curves is important as it provides important constraints on the size of the emitting region in blazar jets via  $R < ct_{\min}\delta(1+z)^{-1}$ . Flux variations on minute time scales have been observed in optical, IR and X-ray regimes. Additionally, in high-energy  $\gamma$ -rays, flux variations as short as minutes have been observed in few sources (Shukla et al. 2018; Meyer et al. 2019; Arlen et al. 2013; Aleksić et al. 2011; Albert et al. 2007; Aharonian et al. 2007). One of the models to explain the observed flux variations in blazars is the shock-in-jet model, which was first proposed by Marscher & Gear (1985) and recently developed further by Böttcher & Dermer (2010). Other models that explain blazar variability include jet-star interaction (Barkov et al. 2012) and the magnetic reconnection models (Giannios 2013).

Blazars have been extensively studied for flux variations at multiple wavelengths, however, the exact mechanisms that cause flux variability are not fully understood yet. Therefore, more information pertaining to the exact physics behind this are needed to enhance our understanding on the flux variability characteristics of blazars. One of the bands of the electromagnetic spectrum where flux variability is less characterised is the  $\gamma$ -ray regime, which is attributable to the paucity of flux variability measurements over a high number of sources. But this band needs to be explored since this is the region where the peak of the high-energy hump of the broad-band SED of blazars lie. Blazars have been studied for their  $\gamma$ -ray variability since the launch of the *Fermi* Gamma-ray Space Telescope in the year 2008. However, most of the time, individual sources were analysed for variability, which, in addition to  $\gamma$ -rays utilises data from other wavelengths (Bonning et al. 2009; Chatterjee et al. 2012; Paliya et al. 2015; Rajput et al. 2019). There are a limited number of studies in the literature that focus on the  $\gamma$ -ray flux variability characteristics of a large sample of blazars. The first study focusing on the  $\gamma$ -ray flux variability of blazars is by Abdo et al. (2010a) who analyse 11 months of data from the *Fermi* Large Area Telescope (LAT) for a total of 106 objects. Similarly, the  $\gamma$ -ray flux variability of high redshift ( $z > 3$ ) blazars has recently been investigated by Li et al. (2018). Quasi-periodic oscillation on year-like time scales have also been reported from the analysis of the long term  $\gamma$ -ray light curves of blazars (Ackermann et al. 2015a; Zhang et al. 2017; Gupta et al. 2019; Bhatta 2019). However, a careful re-analysis of the same data set for a few objects for which quasi-periodicities were reported did not yield any solid evidence as to the existence of year-long periodicities in the  $\gamma$ -ray light curves (Covino et al. 2019; Castignani et al. 2017).

The number of blazars that are known to be emitters of  $\gamma$ -rays has drastically increased since the first study; additionally,  $\gamma$ -ray data spanning more than ten years is now available. The availability of a homogeneous data set on a large sample of blazars enables one to undertake a wide range of analysis in order to characterise  $\gamma$ -ray variability of blazars. Therefore, the main motivation of our present study is to characterise the long term (on month-like time scales)  $\gamma$ -ray variability nature of blazars, which includes characterising the flux variability amplitude and flux variability time scale that could put constraints on blazar emission models, in principle. In addition to characterising variability, we also looked for a correlation in variability with other physical properties of the sources such as the mass of the black hole ( $M_{\text{BH}}$ ) and Doppler factor ( $\delta$ ). A description of the sample and the data used in this work is given in Sect. 2. The details of the data reduction is given in Sect. 3, while the analysis of the data is presented in Sect. 4. The results are summarised in the final section.

## 2. Sample and data

The sample for our study was taken from the third catalogue of AGN detected by *Fermi*-LAT (3LAC; Ackermann et al. 2015b). For this work we selected a total of 1120 sources detected between 100 MeV and 300 GeV with test statistic (TS)  $> 25$ . The TS is a measure of source detection significance and is defined as  $\text{TS} = 2\Delta\log(\text{likelihood})$  between models with and without the source (Mattox et al. 1996). Of these 1120 sources, 639 are BL Lacs and 481 are FSRQs. About 50% of the BL Lacs in our sample have no measured redshift. Excluding those objects, the BL Lacs in our sample have redshifts between 0.03 and 1.72, while the FSRQs have redshifts between 0.16 and 3.10. The distribution of the redshifts of our sample is shown in Fig. 1. By further dividing the sources in the sample that were selected for this study and based on the position of synchrotron peak frequency in their broad-band SED, we have 599 LSPs, 232 ISPs and 289 HSPs. Also shown in Fig. 1 are the distributions of the  $\gamma$ -ray luminosity in the 1–100 GeV range and the  $\gamma$ -ray photon index. The  $\gamma$ -ray luminosities and the photon indices were taken from the 3LAC catalogue<sup>1</sup>. FSRQs are highly luminous and have steeper photon indices in the  $\gamma$ -ray band relative to BL Lacs, which is similar to what is known based on the analysis of three months of data from *Fermi* (Ghisellini et al. 2009).

## 3. Data and reduction

The LAT is the primary instrument on the *Fermi* Gamma-ray Space Telescope, which is designed to measure the energies, directions, and arrival times of  $\gamma$ -rays incident over a wide field of view and it also rejects cosmic-rays from the background. The LAT covers the energy range from below 20 MeV to more than 300 GeV. The LAT has a very wide field of view (Atwood et al. 2009), very good angular resolution and good sensitivity over a large field of view of 2.4 steradian. It's effective area at normal incidence is 9500 cm<sup>2</sup>. The LAT is a pair-conversion Gamma-ray telescope. The primary observing mode of *Fermi* is “scanning” mode. In this mode it covers the full sky in  $\sim 3$  h.

In this work we collected the data from 2008 August 11 to 2017 December 31 for more than nine years within the energy range from 100 MeV to 300 GeV. We analysed the data using the *Fermi* Science Tool version v10r0p5 with the appropriate selections for the scientific analysis of PASS8 data<sup>2</sup>. To analyse the data we used the publicly available python tool *fermipy* (Wood et al. 2017). We considered the data set within the 15° region of interest. In order to avoid background contamination, earth limb were excluded from the analysis (corresponding to the zenith angle cut of more than 90°). The analysis was done by using the maximum likelihood method (gtlike) with the instrument response function “P8R2\_SOURCE\_V6”, the Galactic diffuse model “gll\_iem\_v06.fit” and the isotropic background model “iso\_P8R2\_SOURCE\_V6\_v06.txt”. The good time intervals (GTIs) were created using the criteria “(DATA\_QUAL > 0) &&(LAT\_CONFIG==1)”. We generated 1 month binned light curves for all of the sources in our sample.

## 4. Analysis

### 4.1. Monthly binned light curves

The  $\gamma$ -ray light curves of our sample of sources were generated as per the details found in Sect. 3 for a period of about nine years

<sup>1</sup> <https://www.ssdsc.asi.it/fermi3fgl/>

<sup>2</sup> <http://fermi.gsfc.nasa.gov/ssc/data/analysis/documentation/>

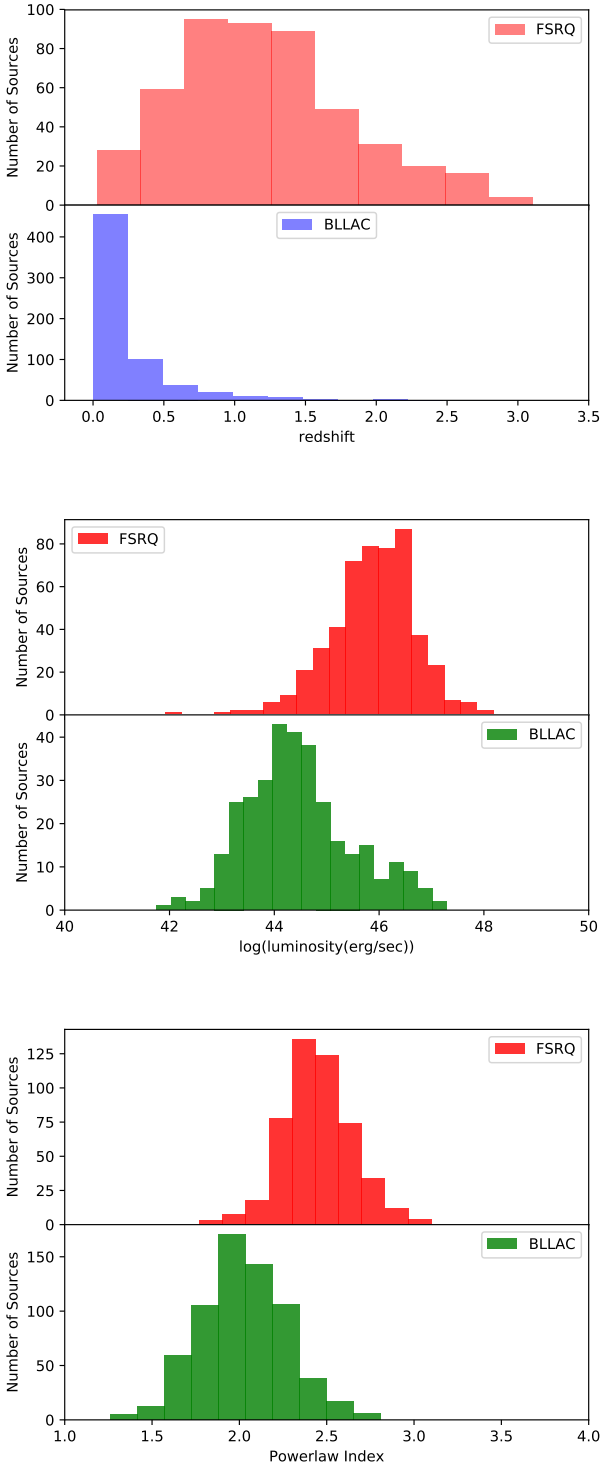


**Fig. 1.** Distribution of redshifts (*top panel*),  $\gamma$ -ray luminosities in the 100 MeV–300 GeV band (*middle panel*) and  $\gamma$ -ray photon indices (*bottom panel*) for FSRQs and BL Lacs analyses in this work for variability.

from 2008 August 11 to 2017 December 31. The light curves were generated with a time binning of one month which results in 114 bins for each light curve. For each interval we calculated the flux and test statistic (TS) values for every source. The TS values were calculated using the maximum likelihood function gtlke. We considered a source to be detected at any epoch if its  $TS > 9$  ( $3\sigma$  detection). At epochs where  $TS < 9$ , the source was considered undetected. In Figs. 2 and 3, we show the light curves

of a few FSRQs and BL Lacs from our sample. It is likely that many light curves do not have flux measurements every month and missing flux points are due to the source’s flux below our detection threshold.

#### 4.2. Flux variability amplitude

To quantify flux variability, we used the fractional root mean square variability amplitude ( $F_{\text{var}}$ ; Vaughan et al. 2003). This is defined as

$$F_{\text{var}} = \sqrt{\frac{S^2 - \sigma_{\text{err}}^2}{\bar{x}^2}} \quad (1)$$

where  $S^2$  is the sample variance and  $\sigma_{\text{err}}^2$  is mean square error. They are given as

$$S^2 = \frac{1}{N-1} \sum_{i=1}^N (x_i - \bar{x})^2 \quad (2)$$

and

$$\sigma_{\text{err}}^2 = \frac{1}{N} \sum_{i=1}^N \sigma_{\text{err},i}^2, \quad (3)$$

Here,  $\sigma_i$  is the statistical uncertainty, to which we added the systematic uncertainty  $\sigma_{\text{sys}} = 0.03\langle x_i \rangle$  in quadrature (Abdo et al. 2009) to get the total error  $\sigma_{\text{err}}$  defined as

$$\sigma_{\text{err}}^2 = \sigma_i^2 + \sigma_{\text{sys}}^2 \quad (4)$$

The uncertainty in  $F_{\text{var}}$  is defined as (Rani et al. 2017)

$$\text{err}(F_{\text{var}}) = \sqrt{\left(\sqrt{\frac{1}{2N}} \frac{\sigma_{\text{err}}^2}{\bar{x}^2 F_{\text{var}}}\right)^2 + \left(\sqrt{\frac{\sigma_{\text{err}}^2}{N}} \frac{1}{\bar{x}}\right)^2} \quad (5)$$

In Fig. 4, the distribution and cumulative distribution of  $F_{\text{var}}$  for FSRQs and BL Lacs are shown. We found mean  $F_{\text{var}}$  values of  $0.47 \pm 0.29$  and  $0.55 \pm 0.33$  for BL Lacs and FSRQs, respectively. A two sample Kolmogorov Smirnov (KS) test shows that the two distributions are indeed different at the 95% level with statistics of 0.15 and a  $p$  value of 0.001. We also sub-divided the sample into different SED classes based on the peak frequency of the low energy synchrotron component in their broad-band SED. The mean  $F_{\text{var}}$  values for the different sub-classes are  $0.54 \pm 0.33$  for LSPs,  $0.45 \pm 0.25$  for ISPs, and  $0.47 \pm 0.33$  for HSPs. The distribution of  $F_{\text{var}}$  values for the different sub-classes are shown in Fig. 5. Ackermann et al. (2011) also find a similar trend of flux variations in the  $\gamma$ -ray band for different classes of blazars. By only Considering BL Lacs, Ackermann et al. (2011), find that variability decreases from LSP to ISP and HSP.

#### 4.3. Duty cycle of variability

We calculated the duty cycle (DC) of variability, including only those sources that have a redshift measurement, in order to determine the fraction of time a particular class of sources shows flux variations. The DC was estimated following Romero et al. (1999) and is given as

$$\text{DC} = 100 \frac{\sum_{i=1}^N Q_i(1/\Delta t_i)}{\sum_{i=1}^N (1/\Delta t_i)} \quad (6)$$

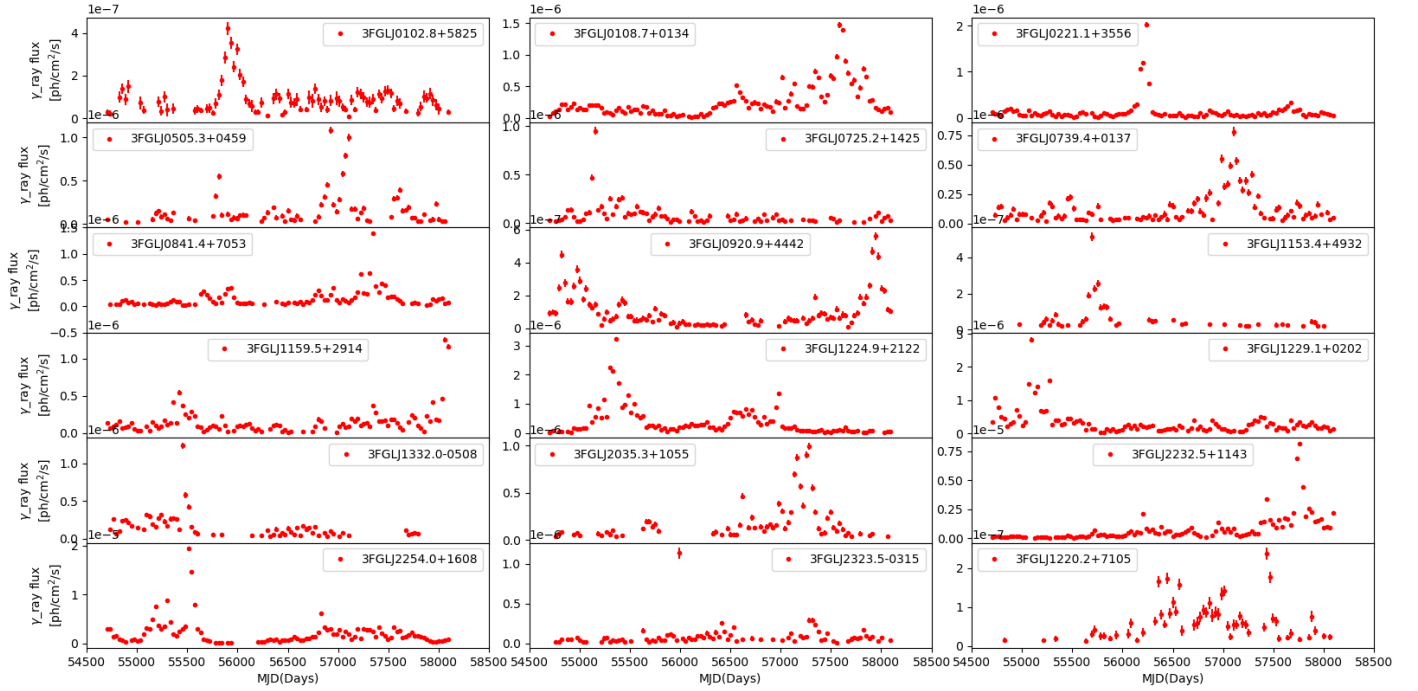


**Fig. 2.** Example light curves for variable FSRQs. The light curves generated on monthly time bins have their integrated fluxes measured between 100 MeV and 300 GeV. The points are the flux values in the monthly bins with  $TS > 9$  (approximately  $3\sigma$ ) and the error bars are their  $1\sigma$  values. The names of the sources are given in each panel.

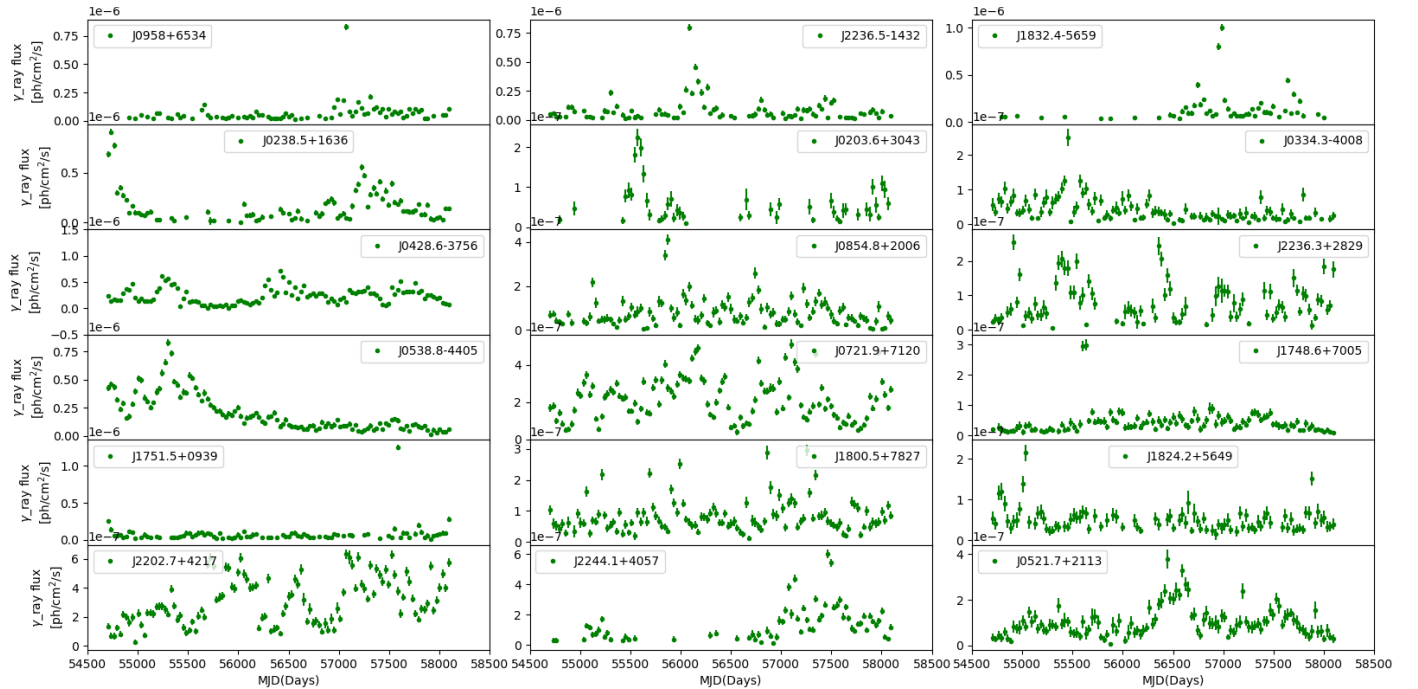


**Fig. 3.** Example monthly binned light curves ( $TS > 9$ ) along with their  $1\sigma$  errors for BL Lacs. The names of the sources are given in each panel. Each point in the light curves refers to flux measured in the 100 MeV–300 GeV band.

where  $\Delta t_i = \Delta t_i(1+z)^{-1}$  is the time in the rest frame of the source,  $N_i = 1$  if a particular source is variable, or else  $N_i = 0$ . For FSRQs, we find a DC of 66%, while for BL Lacs, we find a DC of 36%. For the sub-classes of blazars we find DCs of 65%, 43%, and 36% for LSP, ISP, and HSP blazars, respectively. Thus, LSP sources show a larger DC of  $\gamma$ -ray variability on month-like time scales related to the other classes of blazars.

#### 4.4. Variability time scale

The variability time scale ( $\tau$ ) is a very important parameter that can be deduced from the light curves, which in turn can provide constraints on the physical processes that cause  $\gamma$ -ray flux variations. Since we analyse monthly binned light curves in this work, we were able to probe time scales of the order of months.

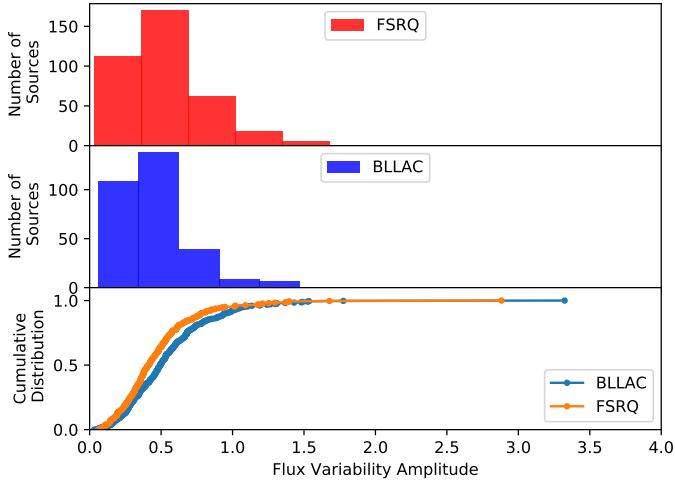


**Fig. 4.** Histogram and cumulative distribution of  $F_{\text{var}}$  for variable FSRQs and BL Lacs studied in this work.

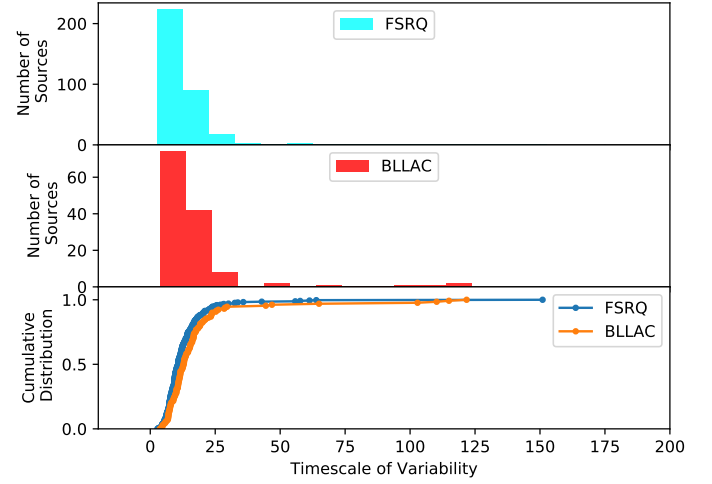


**Fig. 6.** Histogram and cumulative distribution of the time scale of variability (days) for FSRQs and BL Lacs.

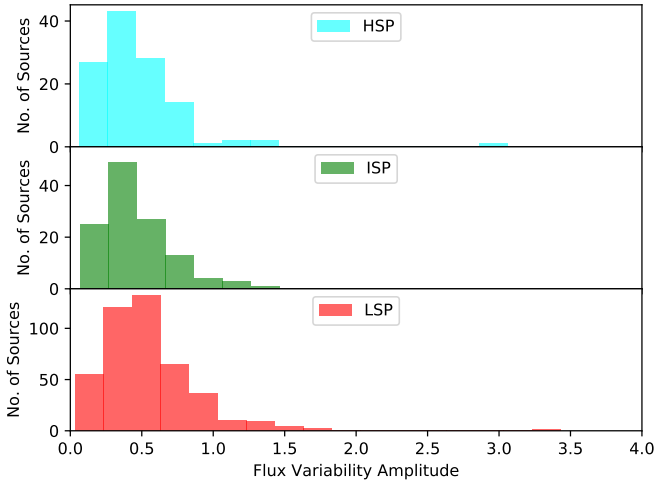


**Fig. 5.** Distribution of  $F_{\text{var}}$  values for variable LSP, ISP and HSP blazars in our sample.

We calculated  $\tau$  of  $\gamma$ -ray flux variability for the sources in our sample that showed  $\gamma$ -ray flux variability following Jorstad et al. (2013)

$$\tau \equiv \Delta t / \ln(S_2/S_1) \quad (7)$$

Here  $S_2$  and  $S_1$  are flux values at a time of  $t_2$  and  $t_1$ , respectively, and  $\Delta t = |t_2 - t_1|$ . In order to estimate  $\tau$ , we considered all possible pairs of flux values that satisfy the conditions (i)  $S_2 > S_1$  and (ii)  $S_2 - S_1 > 3(\sigma_{S_1} + \sigma_{S_2})/2$ , where  $\sigma_{S_2}$  and  $\sigma_{S_1}$  are the uncertainties corresponding to the flux measurements  $S_1$  and  $S_2$ , respectively. Among all of the calculated values of  $\tau$  for a particular source, we considered the minimum  $\tau$  value as the time scale of variability of the source with the  $\gamma$ -ray flux changing by a factor greater than 2. The histogram and cumulative distribution of  $\tau$  for FSRQs and BL Lacs are shown in Fig. 6.

#### 4.5. Ensemble structure function

The variability of AGN can also be described by the structure function (SF), which shows the dependency of variability as a function of time lag (Simonetti et al. 1985). The SF can be calculated for individual AGN that have a light curve with multiple

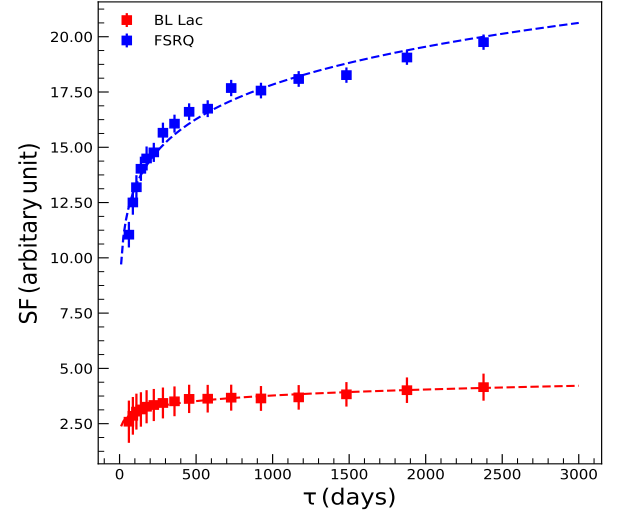


**Fig. 7.** Structure function (SF) against observed frame time lag for BL Lacs (red dots) and FSRQs (blue dots). The dashed lines are the best fits to the SF using Eq. (9).

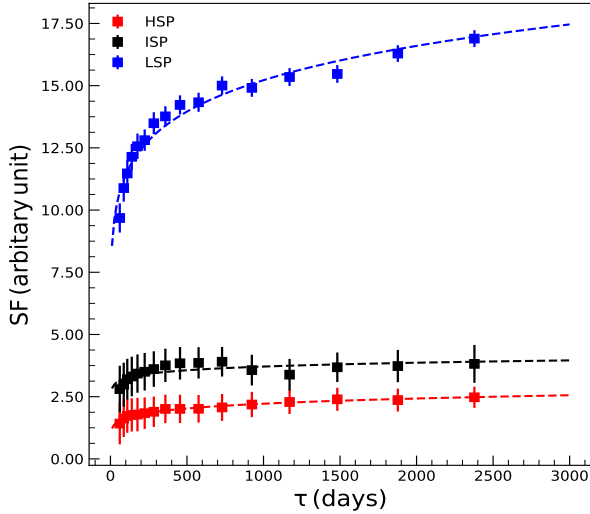
epochs of observations, which takes the magnitude difference for each pair of time lags in a light curve. It can also be calculated for a group of AGN, known as the ensemble structure function, allowing us to obtain the mean variability behaviour of the population that is similar to what has been obtained from the flux variability amplitude. We studied the mean variability of different classes of AGN by using the ensemble structure function following di Clemente et al. (1996)

$$\text{SF} = \sqrt{\frac{\pi}{2} \langle |\Delta m|^2 \rangle - \langle \sigma_n^2 \rangle}, \quad (8)$$

where  $|\Delta m| = m_i - m_j$ , is the magnitude difference between any two epochs ( $i, j$ ) that are separated by time  $\Delta \tau = t_i - t_j$ .  $\sigma_n^2 = \sigma_i^2 + \sigma_j^2$ , which is the square of the uncertainty of the magnitude differences. We note that the majority of our sources do not have redshift measurements in the literature, thus, the SF was calculated in the observed frame. In Fig. 7, we plotted the SF against the observed frame time lag for BL Lacs (red) and FSRQs (blue). The error bar in the SF was calculated via error propagation following Vanden Berk et al. (2004). Figure 7 clearly shows that

**Table 1.** Results of model fits to the structure function using power-law model.

Object class	$S_0$ ( $10^{-8}$ ph $\text{cm}^2$ $\text{s}^{-1}$ )	$\gamma$
BL Lac	$3.92 \pm 0.04$	$0.100 \pm 0.007$
FSRQ	$18.70 \pm 0.20$	$0.132 \pm 0.007$
HSP	$2.33 \pm 0.02$	$0.129 \pm 0.006$
ISP	$3.79 \pm 0.08$	$0.058 \pm 0.014$
LSP	$15.95 \pm 0.16$	$0.124 \pm 0.007$

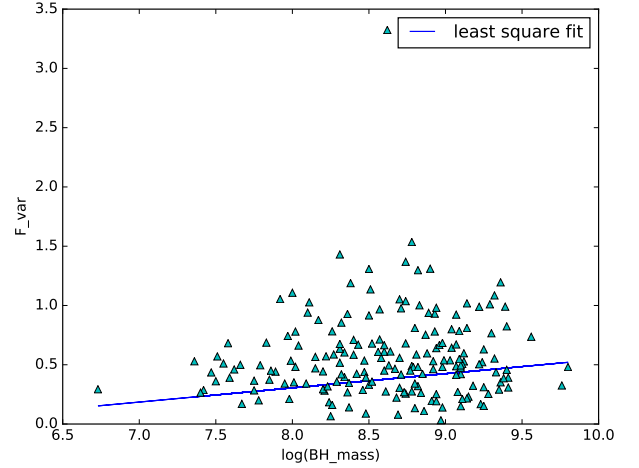

**Fig. 8.** Structure functions for HSP (red), ISP (black) and LSP (blue) blazars. The dashed lines are the best fits to the SF using Eq. (9).

FSRQs are more variable than BL Lacs, which is consistent with the result obtained by  $F_{\text{var}}$  analysis. The SF increases gradually from time lags ranging from one to  $\sim 400$  days and becomes flatter at higher time lags. Such a trend has been noted previously by various authors (Vanden Berk et al. 2004; Welsh et al. 2011; Kozłowski 2016). To characterise the structure function, we fitted the following simple power-law model:

$$\text{SF} = S_0 \times \left( \frac{\Delta\tau}{\tau_0} \right)^\gamma. \quad (9)$$

By adopting  $\tau_0 = 4$  years in the observed frame (Kozłowski 2016) we estimated  $S_0$  and  $\gamma$ . The fitting results are given in Table 1. We note that  $S_0$  is higher in FSRQs than in BL Lacs, suggesting that the former has higher variability than the latter. This is also confirmed from the higher flux variability of the FSRQs compared to BL Lacs. In Fig. 8, we show the SFs of HSP, ISP, and LSP. We find that LSPs have stronger variability followed by ISP and HSP blazars. This is also in agreement with that was obtained from the  $F_{\text{var}}$  analysis.

Based on the analysis of 106  $\gamma$ -ray light curves using 11 months of data from *Fermi*, Abdo et al. (2010b) find FSRQs to show a higher amplitude of  $\gamma$ -ray variability than other AGN classes. Similarly, from an analysis of the sources in the second LAT AGN catalogue, Ackermann et al. (2011) find FSRQs to have more flux variability than BL Lacs. According to Ackermann et al. (2011), the higher variability seen in FSRQs relative to BL Lacs could be attributed to the location of the high-energy peak (in the broad-band SED of blazars) with respect to the *Fermi* band. In the *Fermi* band, FSRQs are observed at energies greater than the inverse Compton peak in


**Fig. 9.** Correlation between  $F_{\text{var}}$  and  $M_{\text{BH}}$  values for FSRQs. The solid line is the unweighted linear least squares fit to the data.

the SED; the observed emission is therefore produced by high-energy electrons with shorter cooling time scales and thereby shows more variations. Alternatively, in the *Fermi* band, BL Lacs are observed at frequencies much lower than the inverse Compton peak, the low-energy electrons have longer cooling time scales, and therefore show low variations. The results obtained in this work on a large sample of blazars having data spanning about nine years is in agreement with the earlier results that were obtained on a smaller sample of blazars with less time coverage (Ackermann et al. 2011; Abdo et al. 2010b).

#### 4.6. $F_{\text{var}}$ , $M_{\text{BH}}$ , and Doppler factor

We searched in the literature for the availability of  $M_{\text{BH}}$  values for the sources analyses for variability here. We could gather  $M_{\text{BH}}$  values (Chen 2018) for a total of 184 FSRQs. In Fig. 9 we show  $F_{\text{var}}$  as a function of  $M_{\text{BH}}$  for FSRQs. There is a weak indication of larger  $\gamma$ -ray flux variations in sources with large  $M_{\text{BH}}$  values. However, linear least squares fit to the data showed an insignificant correlation between  $F_{\text{var}}$  and  $M_{\text{BH}}$  with a linear correlation coefficient of 0.07. Lu & Yu (2001) carried out an analysis of the X-ray flux variations on a composite sample of Seyfert 1 galaxies, quasars and narrow line Seyfert 1 galaxies and found a significant anti-correlation between X-ray variability and  $M_{\text{BH}}$ . Upon the analysis of the long term optical variability characteristics of a large sample of quasars, Zuo et al. (2012) could not find any correlation between  $M_{\text{BH}}$  and variability amplitude, however, other studies have found a correlation between quasar variability and  $M_{\text{BH}}$  (Wold et al. 2007; Bauer et al. 2009), while Kelly et al. (2009) find a negative correlation between  $M_{\text{BH}}$  and quasar variability. Ai et al. (2010) note that the correlation between optical variability and  $M_{\text{BH}}$  vanishes when the Eddington ratio is controlled.

The correlation between  $F_{\text{var}}$  and  $\delta$  for FSRQs and BL Lacs is shown in Fig. 10. We note that  $\delta$  was also collected from Chen (2018). The figure is suggestive of a positive correlation between  $F_{\text{var}}$  and  $\delta$ . However, from the linear least squares fit to the data points, we find no correlation between  $F_{\text{var}}$  and  $\delta$  in both FSRQs and BL Lacs. Any small changes in the jet emission in blazars would get Doppler boosted, leading to the large amplitude of flux variations by the observer. Even though our data sets are indicative of such a correlation, no clear trend could be established.

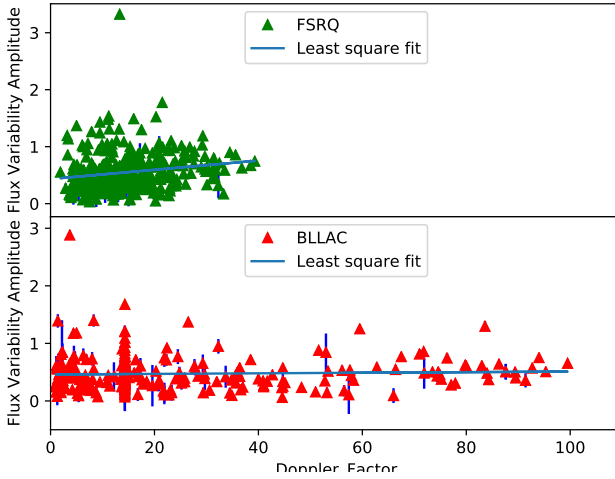


**Fig. 10.** Relation between  $F_{\text{var}}$  and Doppler factor for FSRQs (*top panel*) and BL Lacs (*bottom panel*). Unweighted linear least squares fit to the data are shown as solid lines.

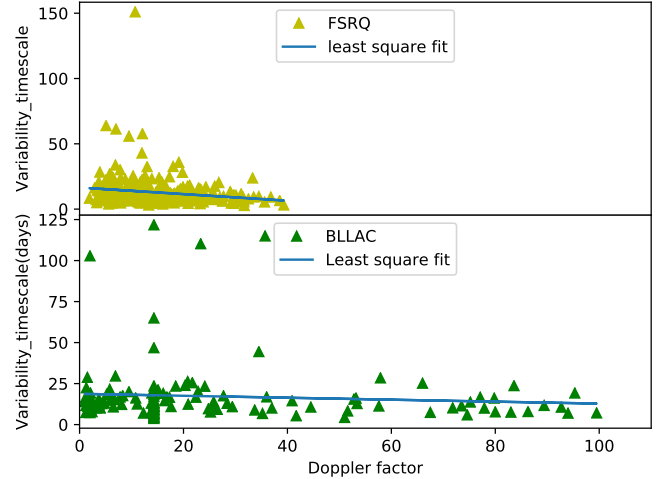


**Fig. 12.** Correlation between time scale of variability and Doppler factor for FSRQs (*top panel*) and BL Lacs (*bottom panel*). Linear least squares fit to the data are shown as solid lines.

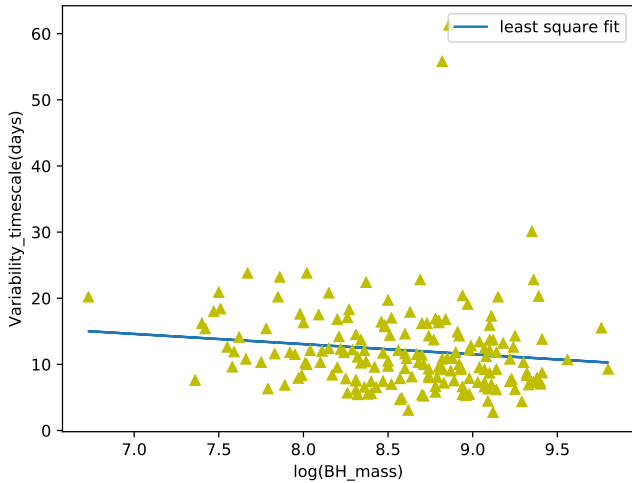


**Fig. 11.** Correlation between time scale of variability and  $M_{\text{BH}}$  for blazars. The solid line is the unweighted linear least squares fit to the data points.

#### 4.7. Time scale of variability, $M_{\text{BH}}$ , and Doppler factor

Knowledge on the time scale of flux variations in blazar light curves is very important as it can provide us important clues as to the physical processes responsible for  $\gamma$ -ray flux variations in blazars. The power spectral density (PSD) is generally used to quantify the time scale of flux variations in blazars, however, we followed the approach given in Eq. (7) to determine the time scale of variability in the monthly binned blazar light curves. From a homogeneous analysis of the blazar light curves, we find that most of the sources analysed in this work have a time scale of variability that is less than 50 days, while few sources have time scales larger than 100 days. From a PSD analysis of the weekly and daily binned  $\gamma$ -ray light curves of 13 blazars spanning about ten years, Ryan et al. (2019) observed two time scales of variability, the longer time scale having a duration of the order of years and the shorter time scale spanning the order of days. According to them, the longer time scales might represent the thermal time scale of the accretion disc, while the shorter time scales may be related to processes in the jet. For most of the sources analysed here, the estimated time scales are of the order

of days, and such time scales could be related to emission processes in the jet (Ryan et al. 2019).

Even though, historically, blazars are separated into FSRQs and BL Lacs based on the width of the emission lines present in their optical spectrum, Ghisellini et al. (2009) postulate a physical distinction between FSRQs and BL Lacs. The PSDs associated with EC, which produces  $\gamma$ -ray emission in FSRQs, and SSC, producing  $\gamma$ -ray emission in BL Lacs, show different break frequencies (Ryan et al. 2019). In such a scenario, different time scales of variability in the  $\gamma$ -ray band are expected. The distribution of  $\tau$  for both FSRQs and BL Lacs are shown in Fig. 4. A KS test indicates that the distribution for each of them is marginally different, with a statistic of 0.18 and  $p$  values of 0.004. We thus noticed a difference in the distribution of the time scales of variability between FSRQs and BL Lacs.

The correlation between  $\tau$  and  $M_{\text{BH}}$  in blazars were found in the X-ray (Chatterjee et al. 2018) and optical (Kelly et al. 2009; MacLeod et al. 2010). In Fig. 11, we show the correlation between  $\tau$  in the  $\gamma$ -ray band against  $M_{\text{BH}}$ . The linear least squares fit to the data yields a low correlation coefficient of  $-0.12$ . We therefore do not find a significant correlation between  $\tau$  and  $M_{\text{BH}}$ . We also do not find any correlation between  $\tau$  and  $\delta$  for both FSRQs and BL Lacs (Fig. 12). Doppler boosting shortens the observed time scale by  $\delta^{-1}$ , and the observed hint (though insignificant) of a negative correlation is a consequence of the effect of  $\delta$  on the time scale of flux variations.

## 5. Summary

In this work we generated one month binned  $\gamma$ -ray light curves for a total of 1120 blazars, comprising 481 FSRQs and 639 BL Lacs to characterise their  $\gamma$ -ray variability with the data collected from *Fermi* for over approximately nine years. This is a systematic study of the  $\gamma$ -ray flux variability using a large sample of blazars. The results of this work are summarised below

1. More than 50% of the blazars studied in this work are found to be variable. Out of the total 639 BL Lacs analyses for variability, 304 sources show variability. Similarly, out of the 481 FSRQs studied for flux variability, 371 are found to be variable. Thus, about 80% of FSRQs are variable, while only about 50% of BL Lacs are variable. We find mean  $F_{\text{var}}$  values of  $0.55 \pm 0.33$  and  $0.47 \pm 0.29$  for FSRQs and BL Lacs,

respectively. Thus FSRQs are more variable than BL Lacs in the  $\gamma$ -ray band. This difference in the  $\gamma$ -ray flux variations between FSRQs and BL Lacs can be explained by the location of the inverse Compton peak in their broad-band SED with respect to the *Fermi* observing band. Among different sub-classes of blazars, LSPs are more variable followed by ISP and HSP blazars. The ensemble structure function analysis also shows that FSRQs are more variable than BL Lacs.

2. FSRQs show the highest DC of variability of 66% relative to BL Lacs that show a DC of 36%.
3. The majority of FSRQs and BL Lacs in our sample show time scales of variability of about 20 days. This time scale could be related to processes in the jets of these sources. The distribution of time scales between FSRQs and BL Lacs are different.
4. Statistically  $F_{\text{var}}$  is not found to be not correlated with either  $M_{\text{BH}}$  and  $\delta$ . Additionally, the time scale of the  $\gamma$ -ray flux variability does not show statistically significant correlation between  $M_{\text{BH}}$  and  $\delta$ .

So our analysis to characterise the  $\gamma$ -ray flux variability on monthly-like time scales of the 1120 blazars for the period of nine years indicates that FSRQs are more variable than BL Lacs, which is also explained by the analysis of the ensemble structure function and the duty cycle. And the time scale of variability and  $F_{\text{var}}$  do not significantly<sup>3</sup> correlate with  $M_{\text{BH}}$  and  $\delta$ .

*Acknowledgements.* This publication makes use of data products from the *Fermi* Gamma-ray Space Telescope and accessed from the Fermi Science Support Center

## References

- Abdo, A. A., Ackermann, M., Ajello, M., et al. 2009, *ApJ*, **700**, 597
- Abdo, A. A., Ackermann, M., Ajello, M., et al. 2010a, *ApJ*, **722**, 520
- Abdo, A. A., Ackermann, M., Agudo, I., et al. 2010b, *ApJ*, **716**, 30
- Ackermann, M., Ajello, M., Allafort, A., et al. 2011, *ApJ*, **743**, 171
- Ackermann, M., Ajello, M., Albert, A., et al. 2015a, *ApJ*, **813**, L41
- Ackermann, M., Ajello, M., Atwood, W. B., et al. 2015b, *ApJ*, **810**, 14
- Aharonian, F., Akhperjanian, A. G., Bazer-Bachi, A. R., et al. 2007, *ApJ*, **664**, L71
- Ai, Y. L., Yuan, W., Zhou, H. Y., et al. 2010, *ApJ*, **716**, L31
- Albert, J., Aliu, E., Anderhub, H., et al. 2007, *ApJ*, **669**, 862
- Aleksić, J., Antonelli, L. A., Antoranz, P., et al. 2011, *ApJ*, **730**, L8
- Arlen, T., Aune, T., Beilicke, M., et al. 2013, *ApJ*, **762**, 92
- Atwood, W. B., Abdo, A. A., Ackermann, M., et al. 2009, *ApJ*, **697**, 1071
- Barkov, M. V., Aharonian, F. A., Bogovalov, S. V., Kelner, S. R., & Khangulyan, D. 2012, *ApJ*, **749**, 119
- Bauer, A., Baltay, C., Coppi, P., et al. 2009, *ApJ*, **696**, 1241
- Bhatta, G. 2019, *MNRAS*, **487**, 3990
- Bonning, E. W., Bailyn, C., Urry, C. M., et al. 2009, *ApJ*, **697**, L81
- Böttcher, M., & Dermer, C. D. 2010, *ApJ*, **711**, 445
- Castignani, G., Pian, E., Belloni, T. M., et al. 2017, *A&A*, **601**, A30
- Chatterjee, R., Bailyn, C. D., Bonning, E. W., et al. 2012, *ApJ*, **749**, 191
- Chatterjee, R., Roychowdhury, A., Chandra, S., & Sinha, A. 2018, *ApJ*, **859**, L21
- Chen, L. 2018, *ApJS*, **235**, 39
- Covino, S., Sandrinelli, A., & Treves, A. 2019, *MNRAS*, **482**, 1270
- di Clemente, A., Giallongo, E., Natali, G., Treves, D., & Vagnetti, F. 1996, *ApJ*, **463**, 466
- Fanaroff, B. L., & Riley, J. M. 1974, *MNRAS*, **167**, 31P
- Ghisellini, G., Maraschi, L., & Tavecchio, F. 2009, *MNRAS*, **396**, L105
- Ghisellini, G., Tavecchio, F., Foschini, L., & Ghirlanda, G. 2011, *MNRAS*, **414**, 2674
- Giannios, D. 2013, *MNRAS*, **431**, 355
- Gupta, A. C., Tripathi, A., Wiita, P. J., et al. 2019, *MNRAS*, **484**, 5785
- Hartman, R. C., Bertsch, D. L., Bloom, S. D., et al. 1999, *ApJS*, **123**, 79
- Jorstad, S. G., Marscher, A. P., Smith, P. S., et al. 2013, *ApJ*, **773**, 147
- Kelly, B. C., Bechtold, J., & Siemiginowska, A. 2009, *ApJ*, **698**, 895
- Kozłowski, S. 2016, *ApJ*, **826**, 118
- Li, S., Xia, Z.-Q., Liang, Y.-F., Liao, N.-H., & Fan, Y.-Z. 2018, *ApJ*, **853**, 159
- Lin, C., Fan, J.-H., & Xiao, H.-B. 2017, *Res. Astron. Astrophys.*, **17**, 066
- Lu, Y., & Yu, Q. 2001, *MNRAS*, **324**, 653
- MacLeod, C. L., Ivezić, Ž., Kochanek, C. S., et al. 2010, *ApJ*, **721**, 1014
- Marscher, A. P., & Gear, W. K. 1985, *ApJ*, **298**, 114
- Matthews, T. A., & Sandage, A. R. 1963, *ApJ*, **138**, 30
- Mattox, J. R., Bertsch, D. L., Chiang, J., et al. 1996, *ApJ*, **461**, 396
- Meyer, M., Scargle, J. D., & Blandford, R. D. 2019, *ApJ*, **877**, 39
- Paliya, V. S., Sahayanathan, S., & Stalin, C. S. 2015, *ApJ*, **803**, 15
- Rajput, B., Stalin, C. S., Sahayanathan, S., Rakshit, S., & Mandal, A. K. 2019, *MNRAS*, **486**, 1781
- Rani, P., Stalin, C. S., & Rakshit, S. 2017, *MNRAS*, **466**, 3309
- Romero, G. E., Cellone, S. A., & Combi, J. A. 1999, *A&AS*, **135**, 477
- Ryan, J. L., Siemiginowska, A., Sobolewska, M., & Grindlay, J. 2019, *ApJ*, **885**, 12
- Shukla, A., Mannheim, K., Patel, S. R., et al. 2018, *ApJ*, **854**, L26
- Simonetti, J. H., Cordes, J. M., & Heeschen, D. S. 1985, *ApJ*, **296**, 46
- The Fermi-LAT Collaboration 2019, *ApJS*, submitted [arXiv:1902.10045]
- Ulrich, M.-H., Maraschi, L., & Urry, C. M. 1997, *ARA&A*, **35**, 445
- Urry, C. M., & Padovani, P. 1995, *PASP*, **107**, 803
- Vanden Berk, D. E., Wilhite, B. C., Kron, R. G., et al. 2004, *ApJ*, **601**, 692
- Vaughan, S., Edelson, R., Warwick, R. S., & Uttley, P. 2003, *MNRAS*, **345**, 1271
- Welsh, B. Y., Wheatley, J. M., & Neil, J. D. 2011, *A&A*, **527**, A15
- Wold, M., Brotherton, M. S., & Shang, Z. 2007, *MNRAS*, **375**, 989
- Wood, M., Caputo, R., Charles, E., et al. 2017, *35th Int. Cosmic Ray Conf.*, **301**, 824
- Zhang, P.-F., Yan, D.-H., Liao, N.-H., & Wang, J.-C. 2017, *ApJ*, **835**, 260
- Zuo, W., Wu, X.-B., Liu, Y.-Q., & Jiao, C.-L. 2012, *ApJ*, **758**, 104

<sup>3</sup> <https://fermi.gsfc.nasa.gov/ssc/data/access/>